Calcium-Triggered Membrane Interaction of the α-Synuclein Acidic Tail†

Shiori Tamamizu-Kato,‡ Malathi G. Kosaraju,‡ Hiroyuki Kato,‡ Vincent Raussens,§ Jean-Marie Ruysschaert,§ and Vasanthy Narayanaswami*,‡

Children's Hospital Oakland Research Institute, 5700 Martin Luther King Jr. Way, Oakland, California 94609, and Center for Structural Biology and Bioinformatics, Structure and Function of Biological Membranes, Université Libre de Bruxelles, CP-206/2, bd. du Triomphe, B-1050 Brussels, Belgium

Received May 11, 2006; Revised Manuscript Received July 6, 2006

ABSTRACT: α-Synuclein (α-syn) is a 140-residue protein that aggregates in intraneuronal inclusions called Lewy bodies in Parkinson's disease (PD). It is composed of an N-terminal domain with a propensity to bind lipids and a C-terminal domain rich in acidic residues (the acidic tail). The objective of this study was to examine the effect of Ca^{2+} on the acidic tail conformation in lipid-bound α-syn. We exploit the extreme sensitivity of the band III fluorescence emission peak of the pyrene fluorophore to the polarity of its microenvironment to monitor subtle conformational response of the α-syn acidic tail to Ca^{2+}. Using recombinant human α-syn bearing a pyrene to probe either the N-terminal domain or the acidic tail, we noted that lipid binding resulted in an increase in band III emission intensity in the pyrene probe tagging the N-terminal domain but not that in the acidic tail. This suggests that the protein is anchored to the lipid surface via the N-terminal domain. However, addition of Ca^{2+} caused an increase in band III emission intensity in the pyrene tagging the acidic tail, with a corresponding increased susceptibility to quenching by quenchers located in the lipid milieu, indicative of lipid interaction of this domain. Taken together with the increased *β*-sheet content of membrane-associated α-syn in the presence of Ca^{2+}, we propose a model wherein initial lipid interaction occurs via the N-terminal domain, followed by a Ca^{2+}-triggered membrane association of the acidic tail as a potential mechanism leading to α-syn aggregation. These observations have direct implications in the role of age-related oxidative stress and the attendant cellular Ca^{2+} dysregulation as critical factors in α-syn aggregation in PD.

α-Synuclein (α-syn)[1] belongs to a family of small, soluble proteins called synucleins (α-, *β*-, and *γ*-synuclein) localized predominantly in neuronal tissues and to a lesser extent in hematopoietic cells and platelets (*1*, *2*). It plays a key role in Parkinson's disease (PD), a neurodegenerative disorder characterized by dramatic losses of dopaminergic neurons in the substantia nigra and in other dementias such as dementia with Lewy body. A hallmark pathological feature of PD is the occurrence of intraneuronal inclusions called Lewy bodies, which are intensely eosinophilic (*3*). The Lewy bodies are composed predominantly of α-syn and lipids, the former deposited as high molecular weight aggregates in a fibrillar state, suggesting loss in solubility or increased protein−protein interactions as putative reasons for aggregation. Two autosomal point mutations in α-syn (A53T and A30P) and overexpression of the wild-type (WT) α-syn pose a high risk for developing PD, although they account for a mere 1% of all PD cases (*4*, *6*); aging appears to be a consistent risk factor in the onset of PD, and there is a consensus about the crucial role for this protein in the pathology of PD, though the exact structural and functional mechanisms of action are not understood.

α-Syn is composed of 140 residues (Figure 1A) and structurally characterized by three modular domains: (a) an N-terminal domain with seven conserved imperfect 11-residue repeats, bearing a propensity to form amphipathic α-helices and to interact with lipid surfaces (*7*), (b) a *β*-amyloid binding domain encoding the non-Abeta component (NAC) of Alzheimer's disease plaques, and (c) a C-terminal tail, characterized by an abundance of negatively charged residues, which binds, among other factors, Ca^{2+} and microtubule-associated proteins 1B (*8*, *9*).

Interestingly, lipid binding of α-syn is mediated via the N-terminal segment, which elicits a binding preference for membranes containing negatively charged phospholipids (*10*), which the weakly anionic C-terminal tail has a natural tendency to repel. Under physiological conditions, α-syn is found in a soluble form in the cytosol and is predominantly disordered (*11*). It is acknowledged that the pathogenesis triggered by α-syn is likely due to structural alterations involving transition from a monomeric unstructured state to

† This work was supported by funding from the Parkinson's Disease Foundation and from the Alzheimer's Association (TLL-03-5281) to V.N., from the National Funds for Scientific Research (Belgium) to V.R., and from the American Heart Association postdoctoral fellowship to S.T.

* Address correspondence to this author. Tel: (510) 428-3885 ext 2965. Fax: (510) 450-7910. E-mail: vnarayan@chori.org.

‡ Children's Hospital Oakland Research Institute.

§ Université Libre de Bruxelles.

[1] Abbreviations: α-syn, α-synuclein; CD, circular dichroism; 5-DSA, 5-DOXYL-stearic acid; IR, infrared; NAC, non-Abeta component; NPM, *N*-(1-pyrene)maleimide; PD, Parkinson's disease; POPA, 1-palmitoyl-2-oleoylphosphatidic acid; POPC, 1-palmitoyl-2-oleoylphosphatidylcholine; TCEP, tris(2-cyanoethyl)phosphine; TFE, 2,2,2-trifluoroethanol; WT, wild type.

10.1021/bi060939i CCC: $33.50
Published on Web 08/16/2006

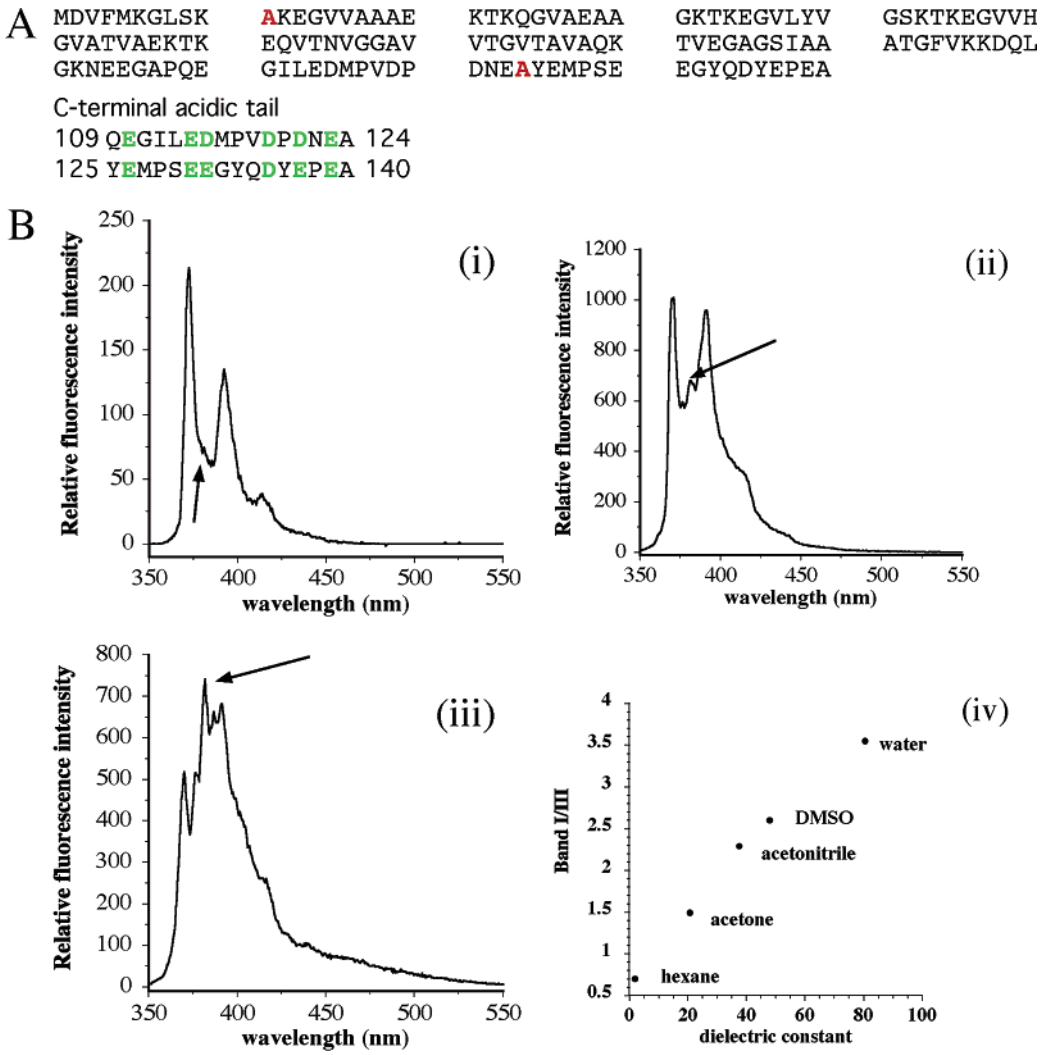

FIGURE 1: Rationale and design of α-syn constructs for site-directed pyrene labeling. Panel A: Primary structure of α-syn. The amino acid sequence of α-syn (residues 1−140) is shown wherein single cysteine residues were substituted at position 11 or 124 in lieu of Ala (red), providing sites for covalent attachment of pyrene tags. The C-terminal tail of α-syn comprises a novel tandem repeat of 16 residues (*14*) between positions 109 and 140 that bear acidic residues (green) at defined intervals. Panel B: Microenvironment-sensitive spectral features of pyrene. Fluorescence emission spectra of free pyrene in (i) aqueous buffer (10 mM HEPES, pH 7.4), (ii) acetone, and, (iii) *n*-hexane. The dielectric constants for these solvents are 80.4, 20.7, and 1.9, respectively, at 20 °C; arrows draw attention to the band III peak at ~387 nm. Fluorescence emission spectra of free pyrene were recorded in various solvents as indicated, and the band I/III ratio was plotted versus the dielectric constant of the solvents (iv). The spectra were recorded at an excitation wavelength of 340 nm.

a *β*-sheet filamentous state (*12*), with a partially folded intermediate likely playing a critical role in the aggregation process (*13*).

Functionally, α-syn has also been implicated in dopamine and Ca^{2+} signaling, with the C-terminal segment likely involved in the Ca^{2+} binding process (*14*, *15*). Other putative functions include a role in neurotransmitter release from presynaptic vesicles and modulation of presynaptic vesicle pool size, plasticity, and recycling via the dopamine transporter (*16*) and other calcium-mediated roles (*14*, *15*, *17*, *18*). A possible clue to the role of α-syn may lie in the fact that aging is consistently associated as a risk factor for PD. Inevitably, oxidative stress appears to be a necessary accompaniment of the normal aging process and is closely associated with the neurobiology of aging, including neurodegeneration in Alzheimer's disease and PD (*19*). In addition, oxidative stress is intrinsically linked to Ca^{2+} dysregulation, with documented reports of increase in Ca^{2+} influx and intracellular Ca^{2+} leading to a severe disruption of the normal cellular processes (*20*−*23*). This further implies that the presynaptic terminal, with an abundance of α-syn, lipids, and high local concentration of Ca^{2+}, is a crucial site for initiating pathogenesis of PD.

In this study we propose that Ca^{2+} triggers a conformational restructuring of the acidic tail of α-syn that is anchored to the membrane surface via its N-terminal domain. We employ site-directed fluorescence labeling of recombinant human α-syn to evaluate the relative spatial disposition of its N-terminal and C-terminal segments in lipid-free and lipid-bound states. Our studies suggest that Ca^{2+} either bridges α-syn to the membrane, possibly by coordinating with the negative charge on the α-syn acidic tail and the acidic headgroups in the phospholipid bilayer, or facilitates this segment to traverse the membrane bilayer.

MATERIALS AND METHODS

Materials. *N*-(1-Pyrene)maleimide (NPM), tris(2-cyanoethyl)phosphine (TCEP), and *N*-(1-pyrenesulfonyl)-1,2-hexadecanoyl-*sn*-glycero-3-phosphoethanolamine were obtained

from Molecular Probes Invitrogen (Carlsbad, CA). 5-DOXYL-stearic acid (5-DSA), 1-palmitoyl-2-oleoyl-*sn*-glycero-3-phosphocholine (POPC), and 1-palmitoyl-2-oleoyl-*sn*-glycero-3-phosphate (POPA) were obtained from Avanti-Polar Lipids (Alabaster, AL). 2,2,2-Trifluoroethanol (TFE) and free pyrene were obtained from Sigma (St. Louis, MO). All other chemicals and solvents were of analytical grade.

α-Synuclein Constructs and Protein Expression. Human wild-type (WT) α-syn was subcloned into a pTYB1 expression vector to facilitate purification of the recombinant protein using the IMPACT-CN system (New England BioLabs, Beverly, MA) as described earlier (*24*). Site-directed mutagenesis was carried out to generate single cysteine-containing constructs of α-syn, which otherwise lacks cysteine residues. Cysteine residues were substituted at position 11 or position 124, yielding A11C- or A124C-α-syn, respectively. Single Cys variants were generated by PCR-based site-directed mutagenesis, carried out by mismatch amplification using two sequential PCRs by the Expand High Fidelity PCR system (Roche Applied Science). All constructs were sequenced to confirm that there were no undesired mutations. Recombinant WT-, A11C-, and A124C-α-syn were expressed in *Escherichia coli* as a fusion protein, followed by DTT-induced intein-mediated self-cleavage on a chitin matrix.

Site-Specific Pyrene Labeling. A11C- and A124C-α-syn were initially preincubated with a 5-fold molar excess of TCEP for 1 h at 37 °C to reduce existing intermolecular disulfide bonds. This was followed by incubation with a 5-fold molar excess of NPM at 37 °C for 4 h (*25*, *26*). A Sephadex G-75 gel filtration column was used to remove the excess unbound TCEP and NPM.

Fluorescence Measurements. Fluorescence spectra were recorded on a Perkin-Elmer LS50B fluorometer. Unless otherwise specified, 10 mM HEPES buffer, pH 7.4, was used in all of the fluorescence experiments. When the effect of Ca^{2+} was followed, POPC/POPA/α-syn complexes were incubated with 0, 0.1, 0.2, 0.5, 1.0, or 2.0 mM $CaCl_2$ as specified for 16 h at 24 °C. Fluorescence measurements were carried out directly on the samples with a slit width of 3 nm for both the excitation and emission monochromators. Emission spectra were collected from 350 to 600 nm by setting the excitation wavelength at 340 nm.

Effect of TFE and pH Alteration on Pyrene-A11C/α-Syn and Pyrene-A124/α-Syn Fluorescence. Fluorescence emission spectra of 4 μg of pyrene-A11C/α-syn or pyrene-A124C/α-syn in the absence or the presence of varying concentrations of TFE were recorded. The final TFE concentrations ranged from 0% to 50% (v/v) in the incubation mixtures. The effect of pH was evaluated by recording emission spectra of 4 μg of pyrene-labeled α-syn in 50 mM sodium phosphate buffer (pH 6.0, 7.0, or 8.0) or 50 mM sodium acetate buffer (pH 3.0, 4.0, and 5.0).

Preparation and Characterization of POPC/POPA/Pyrene-Labeled α-Syn Complexes. Small unilamellar vesicles (SUVs) of POPC/POPA were prepared by sonication. Ten milligrams each of POPC and POPA [1:1 (w/w)] was initially dissolved in chloroform and then dried under a stream of N_2 gas to make a thin film. The thin film was incubated in 20 mM phosphate buffer (pH 7.4) for 5 min at 42 °C, vortexed, and sonicated for 3 h at 24 °C in a bath sonicator. α-Syn (1 mg of protein) was incubated with the SUVs for 16 h at 24 °C. Superose 6 gel filtration column chromatography was performed at a flow rate of 0.3 mL/min to separate the POPC/POPA/α-syn complexes from unbound protein and protein-free SUV. The molecular mass of the POPC/POPA/α-syn complexes was calculated using thioesterase II and bovine serum albumin as standards. The phospholipid and protein content of the complexes was estimated using the phospholipid assay kit (Wako Chemicals GmbH) and the DC protein assay kit (Bio-Rad), respectively, to calculate the lipid:protein ratio. Additionally, native PAGE of the isolated complexes was carried out to evaluate the molecular mass and size of the particle on a 4−20% gradient gel for 20 h at 150 V and stained with Amido Black. The molecular masses of the POPC/POPA/α-syn complexes were calculated from a calibration curve using the following standards: thyroglobulin, 669 kDa; ferritin, 440 kDa; catalase, 232 kDa; lactate dehydrogenase, 140 kDa.

Quenching Studies. To verify the location of the fluorophores in or proximal to the phospholipid bilayer, fluorescence quenching analysis was performed with POPC/POPA/pyrene-A11C/α-syn or POPC/POPA/pyrene-A124C/α-syn in the absence and the presence of 1 mM Ca^{2+} with varying 5-DSA concentrations. The rationale behind this analysis is that fatty acids partition directly into the membrane bilayer, and by comparing the quenching constants, we can estimate the relative location of the fluorophores in the variants with respect to the membrane. The DOXYL group (quenching moiety) is located at position C-5 along the fatty acyl chain in 5-DSA. Aliquots of 5-DSA (13 mM stock in DMSO) were added directly to POPC/POPA/α-syn complexes [keeping the final concentration of DMSO ≤2% (v/v)], and the fluorescence intensities were measured at 375 nm following equilibration for 5 min. The effective Stern−Volmer quenching constants (K_{SV}) were calculated employing the Stern−Volmer equation $F_0/F = 1 + K_{SV}[Q]$, where F_0 and F are the fluorescence intensities in the absence and the presence of varying quencher concentrations, respectively, and [Q] is the quencher concentration (*26*, *27*).

Circular Dichroism Spectroscopy. Prior to CD and infrared (IR) measurements, the POPC/POPA/α-syn complexes were dialyzed against 5 mM HEPES, pH 7.4, and then the Ca^{2+} concentration was adjusted using a stock solution of $CaCl_2$. The samples were incubated for 16 h at 24 °C and the CD spectra recorded using a 0.05 cm cuvette on a Jasco-710 spectropolarimeter maintained at 24 °C. Four scans, recorded from 185 to 260 nm at 50 nm/min with a 1 nm slit width and a time constant of 0.5 s for a nominal resolution of 1.7 nm, were averaged. Spectra were analyzed for secondary structure using the CDPRO analysis software (*28*).

Infrared Spectroscopy. IR spectra were recorded on a Bruker EQUINOX 55 infrared spectrophotometer equipped with a reflectance accessory. The internal reflection element was a diamond crystal (2 × 2 mm) with an aperture angle of 45° yielding a single internal reflection. The spectra were recorded at a nominal resolution of 2 cm^{-1} and averaged over 128 accumulations to improve the signal/noise ratio. The spectrophotometer was continuously purged with dried air. All measurements were made at 24 °C.

RESULTS AND DISCUSSION

Rationale and Design. The objective of this study was to examine the lipid-triggered switch in the conformational

disposition of α-syn, with respect to its N-terminal domain and C-terminal acidic tail, and their response to Ca^{2+}. The N-terminal domain and acidic tail were selectively monitored by substituting single cysteine residues at position 11 or 124 of α-syn, respectively (Figure 1, panel A). Since WT α-syn lacks Cys residues, the introduced site was unique, allowing us to covalently attach pyrene maleimide and to monitor the individual domains. Pyrene maleimide was the fluorescent probe of choice as it bears a long fluorescence lifetime (~100 ns) and high extinction coefficient (40000 cm^{-1} M^{-1}) (*29*); importantly, it exhibits a distinct spectral feature that allows us to monitor the proposed Ca^{2+}-induced conformational alteration, namely, the Py scale. Unique to pyrene, this feature is extremely sensitive to the changes in the hydrophobicity of the microenvironment.

The Py scale is based on the $\pi-\pi^*$ emission spectrum of the pyrene monomer, which exhibits five major well-resolved vibronic bands between 370 and 430 nm, progressively labeled as bands I, II, III, IV, and V. Since the electronic and vibronic states are coupled, the first vibronic band (0−0 transition, band I, ~375 nm) displays enhanced emission intensity with increasing solvent polarity compared to the third band (0−2 transition, band III, ~385 nm). The ratio of intensity between band I and band III (band I/band III) is sensitive to the polarity in the microenvironment of the probe (*30*). By calculating the ratio (I/III) in different solvents, the Py scale of solvent polarity has been established in an empirical process, and the I/III values are generally referred as Py values (*31*, *32*), which has been widely employed to assess changes in the polarity of the environment of the probe (*30*, *33*).

The potential application of the Py scale in studying protein/membrane interaction is illustrated by recording the fluorescence emission spectra of pyrene in solvents of widely ranging dielectric constants: aqueous buffer (10 mM HEPES, pH 7.4), acetone, and hexane (Figure 1, panel B, i−iii, respectively). In aqueous buffer (dielectric constant: 80.4) well-defined vibronic bands at 375 and 395 nm were noted, while band III at 387 nm is barely visible (Py value = 3.28). In acetone (dielectric constant: 20.7) band III (385 nm) becomes visible as a distinct peak (Py value = 1.44), while in hexane (dielectric constant: 1.9), band III (382 nm) is pronounced and displays a dramatically increased intensity (Py value = 0.68), indicative of a highly nonpolar environment in the latter. A plot of Py value versus dielectric constant for various solvents (Figure 1, panel B, iv) shows that small changes in the band I/III ratio can be reflective of large differences in the polarity of the probe microenvironment. Thus, by following the intensity of band III relative to band I, it is possible to interpret the nature of the microenvironment of the pyrene probe. We take advantage of these unique spectral properties of pyrene as a reliable indicator to monitor the spatial positioning of the N-terminal and C-terminal segments of α-syn with respect to the membrane, an approach successfully employed to assess conformational modulations and microenvironment polarity in other proteins (*31*−*34*).

Pyrene Labeling of α*-Syn.* Following expression and purification on an affinity matrix, the final α-syn preparations were ~98% pure as judged by SDS−PAGE and existed predominantly as a dimer (not shown). The protein was reduced prior to labeling with NPM (*25*), and the stoichiometry of labeling was calculated to be ~1 pyrene/α-syn molecule, using the extinction coefficient for pyrene ϵ_{340} = 40000 M^{-1} cm^{-1}. Further, CD analysis of the unlabeled and pyrene-labeled single Cys variants revealed the presence of a predominantly unstructured protein comparable to WT α-syn, consistent with previous reports (*35*) indicating that the Cys substitution did not alter the overall secondary structural characteristics of α-syn.

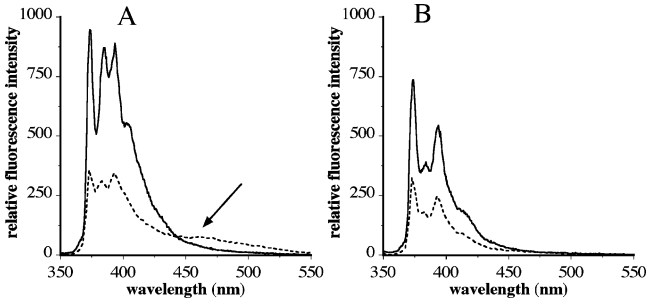

FIGURE 2: Fluorescence emission spectra of pyrene-labeled lipid-free and lipid-bound α-syn. Panel A: Emission spectra of 10 μg/mL pyrene-A11C/α-syn (dotted line) and 4 μg/mL POPC/POPA/pyrene-A11C/α-syn (solid line). The arrow draws attention to the excimer peak at ~460 nm in the spectrum of lipid-free protein. Panel B: Emission spectra of 10 μg/mL pyrene-A124C/α-syn (dotted line) and 4 μg/mL POPC/POPA/pyrene-A124C/α-syn (solid line). The spectra were recorded at an excitation wavelength of 340 nm.

Fluorescence Characteristics of Lipid-Free α*-Syn Variants.* The fluorescence emission spectra of pyrene-A11C/α-syn and pyrene-A124C/α-syn were recorded at 10 μg/mL in 10 mM HEPES, pH 7.4, following excitation at 340 nm (Figure 2, panels A and B, respectively). In both cases (dotted lines), structured fluorescence emission with well-defined vibronic bands was noted. In the case of pyrene-A11C/α-syn, pyrene fluorescence emission attributed to monomeric moieties (373, 385, 395 nm, with a shoulder at 415 nm) was noted. The arrow at 460 nm in panel A is indicative of a possible dimeric pyrene (called excimer) (*36*−*38*) in the case of A11C/α-syn but not in pyrene-A124C/α-syn. The excimer emission peak was not observed at concentrations of <2 μg/mL for pyrene-A11C/α-syn. The concentration-dependent appearance of excimer emission in pyrene-A11C/α-syn, but not in pyrene-A124C/α-syn, is an indication that neighboring α-syn molecules are spatially proximal (<10 Å) primarily at the N-terminal domain. This observation may be attributed to the lipid-seeking nature of the N-terminal domain, which is satisfied by protein−protein interactions, and to the abundance of negatively charged residues at the C-terminal end, which likely causes repulsion in a lipid-free state.

Characterization of Lipid-Bound α*-Syn Complexes.* In the next step, α-syn was allowed to interact with phospholipid vesicles [20:1 lipid:protein (w/w) ratio] (*10*). The lipid-bound α-syn was separated from the lipid-free protein and protein-free vesicles by gel filtration. On the basis of earlier studies (*10*, *39*, *40*) that demonstrate a critical requirement for acidic phospholipids in order for α-syn to interact with lipid surfaces, we employed POPC:POPA in a weight ratio of 1:1. On the basis of the documented effect of Ca^{2+} in inducing fusion of vesicles containing 1-palmitoyl-2-oleoyl-*sn*-glycero-3-[phospho-L-serine] (POPS), POPA was preferred as the negatively charged phospholipid in our mixtures. Initial characterization of POPC/POPA/α-syn complexes prepared

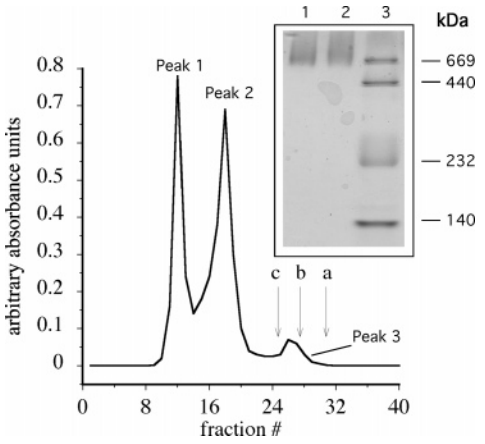

FIGURE 3: Size exclusion chromatography of POPC/POPA/α-syn complexes. The POPC/POPA/WT/α-syn complex (0.5 mg of protein) was applied on a Superose 6 FPLC system (30 cm × 1 cm) with the flow rate set at 0.3 mL/min. Fractions under peak 1 were comprised of protein-free vesicles, while those under peak 3 were lipid-free protein. Fractions containing α-syn and phospholipids (peak 2) were pooled, concentrated, and used as such. The molecular mass of the complexes was estimated using thioesterase II, bovine serum albumin monomer, and bovine serum albumin dimer as standards with molecular masses of 30, 56, and 112 kDa, respectively (indicated by arrows a, b, and c, respectively). Inset: Native PAGE analysis of POPC/POPA/α-syn complexes. Lipid-bound α-syn variants were isolated by gel filtration as described above. POPC/POPA/A11C/α-syn (lane 1) and POPC/POPA/A124C/α-syn (lane 2) complexes (20 μg of protein) were electrophoresed on a 4−20% acrylamide gradient gel for 24 h at 150 V and stained with Amido Black B. Native PAGE standard is shown in lane 3.

under our conditions was carried out by gel filtration and native PAGE analyses. Gel filtration experiments of the POPC/POPA/α-syn complexes by the Superose 6 FPLC system (using thioesterase II, bovine serum albumin monomer, and bovine serum albumin dimer as standards with molecular masses of 30, 56, and 112 kDa, respectively) yielded a molecular mass of ~226 kDa (Figure 3). However, native PAGE analysis of POPC/POPA/α-syn complexes (A11C- and A124C/α-syn) revealed a molecular mass of ~670 kDa (Figure 3, inset). Particle composition analysis of POPC/POPA/α-syn complexes was carried out by protein and phospholipid assays, which yielded a lipid:protein molar ratio of 70:1.

Fluorescence Emission Spectra of Lipid-Bound Pyrene-Labeled α-Syn Variants. The fluorescence emission spectra of POPC/POPA/pyrene-A11C/α-syn and POPC/POPA/pyrene-A124C/α-syn complexes are represented in Figure 2, panels A and B, respectively (solid lines). There were three dramatic differences in the spectral features of the lipid-bound variants when compared to the corresponding lipid-free spectra: (i) a large increase in the fluorescence quantum yield upon lipid binding, ~4-fold in the case of pyrene-A11C/α-syn and ~3-fold for pyrene-A124C/α-syn (note: spectra of the lipid-bound samples were recorded with 4 μg of protein compared to 10 μg for the lipid-free protein), (ii) loss of the distinct excimer emission in the case of pyrene-A11C/α-syn, with no changes noted for pyrene-A124C/α-syn, and (iii) large differences in the monomer emission profile of lipid-bound pyrene-A11C/α-syn, with no changes noted for pyrene-A124C/α-syn. In the lipid-free state, the intensity of band I is higher than that of band III (band I/III, 1.2) for pyrene-A11C/α-syn, while in the lipid-bound state, an increase was noted in the relative intensity of band III compared to that of band I, reflected as a decrease in ratio of band I/band III to 1.0. This is a clear indication of the relative hydrophobic microenvironment in the vicinity of position 11, i.e., the N-terminal domain of α-syn, suggesting a direct interaction with the lipid surface, consistent with earlier studies (*10*, *41*). On the other hand, the intensity of band I remained significantly higher compared to that of band III in both lipid-free and lipid-bound states for A124C/α-syn (ratio of 1.89 and 1.99, respectively). The 3-fold increase in quantum yield induced by lipid association of pyrene-A124C/α-syn is likely due to the overall restraint imposed on the protein molecule by lipid interaction of its N-terminal domain. Although an alternate interpretation for this observation could be possible tail−tail interaction of neighboring α-syn, we believe that the net negative charge of this segment is likely to prevent such an interaction. This suggests that α-syn is likely anchored to the lipid surface via the N-terminal segment, with the acidic tail "flapping" in the aqueous milieu surrounding the lipid surface.

Effect of Altering pH on the α-Syn Conformation. We rationalized that the acidic tail remains unbound in lipid-bound α-syn, due to charge−charge repulsion between the acidic residues in the C-terminal segment and the acidic headgroup of phosphatidic acid in the vesicles. If so, a decrease in the solution pH should cause an increase in the net hydrophobicity of the C-terminal tail due to protonation of the acidic side chains, thereby facilitating binding interaction with the lipid surface. To verify this, the effect of altering pH on the fluorescence emission spectra of POPC/POPA/pyrene-A11C/α-syn and POPC/POPA/pyrene-A124C/α-syn was monitored (Figure 4, panels A and B, respectively). In the case of POPC/POPA/pyrene-A11C/α-syn, decreasing the pH had no effect on the overall fluorescence emission characteristics compared to the profile recorded at pH 7.0 (Py value of 1.01 at all pH values). However, in the case of POPC/POPA/pyrene-A124C/α-syn, decreasing the pH caused a progressive increase in the emission intensity of band III at 387 nm (Py values of 1.99, 1.25, and 0.93 at pH 7.0, 5.0, and 4.0, respectively), indicative of a relatively more hydrophobic environment as a result of membrane interaction by the C-terminal end of α-syn. We exclude possible changes in fluorescence due to direct pH-related effects on the headgroup of POPA (*42*) since the changes we noted were specific for pyrene-A124C/α-syn. The above study indicates that the acidic tail conformation likely responds to changes in the microenvironment, leading us to examine the effect of factors likely to interact with residues in the C-terminal segment of α-syn, such as Ca^{2+}. Ca^{2+} is undisputedly a significant regulatory player in several cellular and biochemical events, especially in the neurons (*43*, *44*).

Effect of Ca^{2+} on the Acidic Tail Disposition with Respect to the Membrane. We assessed the effect of varying Ca^{2+} concentration (0.1, 0.2, 0.5, and 1.0 mM $CaCl_2$) on the spatial disposition of the α-syn acidic tail by comparing the fluorescence emission profile of POPC/POPA/pyrene-A11C/α-syn and POPC/POPA/pyrene-A124C/α-syn following incubation with Ca^{2+} (Figure 5, panels A and B, respectively) (only 0, 0.5, and 1.0 mM Ca^{2+} are shown). The presence of Ca^{2+} had no significant effect on the fluorescence emission profile for POPC/POPA/pyrene-A11C/α-syn, with the Py scale remaining unchanged at ~1.0 at all concentrations

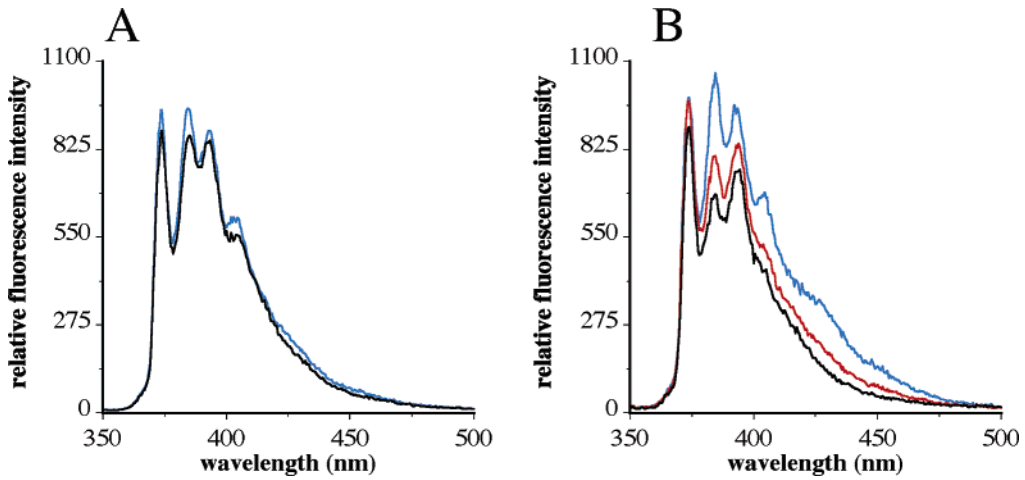

FIGURE 4: Effect of altering pH on α-syn conformation. Fluorescence emission spectra of POPC/POPA/pyrene-A11C/α-syn were recorded at pH 7.0 (black) and pH 4.0 (blue) (panel A). Fluorescence emission spectra of POPC/POPA/pyrene-A124C/α-syn (panel B) were recorded at pH 7.0 (black), pH 5.0 (red), and pH 4.0 (blue). Lipid-bound pyrene-labeled α-syn variants were prepared as described under Materials and Methods. Spectra of complexes were recorded using 4 μg of protein at an excitation wavelength of 340 nm.

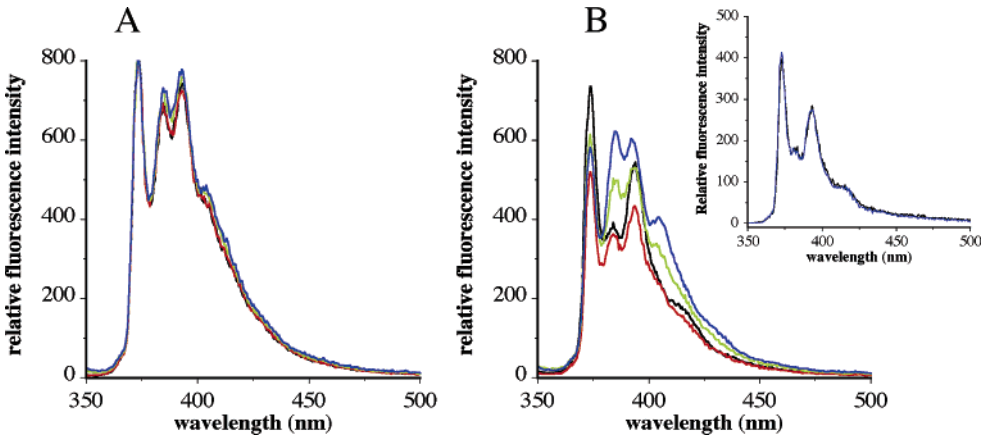

FIGURE 5: Effect of Ca^{2+} on the fluorescence emission of lipid-bound pyrene-labeled α-syn. Fluorescence emission spectra of POPC/POPA/pyrene-A11C/α-syn (panel A) and POPC/POPA/pyrene-A124C/α-syn (panel B) were recorded in the absence (black) and the presence of 0.1 mM (red), 0.5 mM (green), and 1.0 mM (blue) Ca^{2+} at an excitation wavelength of 340 nm. Representative spectra are shown from about 10 different experiments. Inset in panel B: Effect of 0 (black) and 1 mM Ca^{2+} (blue) on fluorescence emission characteristics of *lipid-free* pyrene-A124C/α-syn.

studied. However, in the case of A124C/α-syn a significant increase in the relative intensity of the 387 nm peak compared to 375 nm was noted, reflected as a decrease in the Py scale to 1.4 in the presence of Ca^{2+} at 0.5 mM or higher concentrations (from 1.99 in the absence of Ca^{2+}). The change in Py scale is indicative of a more hydrophobic microenvironment in the vicinity of position 124. This suggests that the acidic tail of α-syn, which had hitherto remained unbound in the absence of Ca^{2+}, is likely interacting with the lipid surface in its presence. The membrane apposition of the acidic tail was unique to Ca^{2+}, as other divalent cations such as Mg^{2+} (or monovalent cations such as Na^{+}) did not elicit a similar response (data not shown). These studies indicate that the effect is Ca^{2+}-dependent and not due to any nonspecific effect of the pyrene fluorophore.

To verify that the Ca^{2+}-induced changes noted in the emission spectra of POPC/POPA/pyrene-A124C/α-syn are not due to Ca^{2+} bridging of the acidic tails between neighboring α-syn moieties, we checked the effect of Ca^{2+} on fluorescence emission characteristics of *lipid-free* pyrene-A124C/α-syn (Figure 5, panel B, inset). There were no changes in the emission profile, suggesting that the changes noted are not due to apposition of neighboring acidic tails of α-syn molecules.

To independently confirm that Ca^{2+} induces membrane juxtaposition of the acidic tail, we attempted to quench the fluorescence emission of pyrene located in the C-terminal segment of α-syn by membrane-based quenchers such as 5-DSA. The nitroxyl moiety is an excellent quencher of fluorescence, and this quenching property has been routinely employed to probe the location of fluorophores in membranes (*25*, *45*−*47*). 5-DSA was added in incremental amounts to POPC/POPA/pyrene-A124C/α-syn in the absence of Ca^{2+}. Since the concentrations used are well below the critical micelle concentration of DSA, we believe that it readily partitions into the membrane. Fluorescence quenching was followed at 375 nm at various quencher concentrations, and the effective Stern−Volmer quenching constant (K_{SV}) was calculated to be $(17.1 \pm 3.7) \times 10^{-3}$ M^{-1}. In the presence of 1 mM Ca^{2+}, the apparent K_{SV} increased to $(36.5 \pm 5.6) \times 10^{-3}$ M^{-1}. To evaluate the status of the probe at the N-terminal end under identical conditions, similar quenching analysis was carried out for POPC/POPA/pyrene-A11C/α-syn in the absence and the presence of Ca^{2+}, yielding K_{SV}

values of $(20.6 \pm 5.3) \times 10^{-3}$ and $(64.7 \pm 23.1) \times 10^{-3}$ M^{-1}, respectively. When considered in conjunction with the response of the fluorescence emission peak at 387 nm, these data indicate that the pyrene fluorophore at position 124 is closer to the membrane surface in the presence of Ca^{2+}, compared to its location in the absence of Ca^{2+}; on the other hand, the fluorophore at position 11 was already close to the membrane surface in the absence of Ca^{2+} but relocated to a deeper site in its presence. Although DSA has been shown to bind other proteins (*48*), we exclude this possibility in the present study since 5-DSA was added to POPC/POPA/α-syn complexes and not to lipid-free α-syn. Further, since α-syn does not appear to bear high-affinity binding of fatty acids to specific sites as in fatty acid binding proteins (*49*), we believe that the added DSA partitions directly into the membrane bilayer.

In parallel studies, CD and IR analysis of lipid-bound WT α-syn was carried out in the presence of varying concentrations of Ca^{2+} to assess its effect on the secondary structure of lipid-bound protein. In the absence of Ca^{2+}, lipid-bound α-syn (both unlabeled and pyrene-labeled) adopts a helical structure, consistent with other reports (*10*); this shows that pyrene labeling does not alter the overall structural behavior of α-syn. Comparison of the CD profile of α-syn in the presence of 50% TFE and in the lipid-bound state reveals an interesting difference: the ratio of molar ellipticities at 222 and 208 nm is ~1.0 in the lipid-bound state in contrast to a ratio of <1.0 in the presence of TFE. The absorbance at 222 and 208 nm is attributed to $n-\pi^*$ and $\pi-\pi^*$ transitions, respectively, with the 208 nm absorbance (which polarizes parallel to the helical axis) sensitive to the curvature of the helix (*50*). The α-helical and β-sheet content was 53% and 11%, respectively, in the absence of added Ca^{2+}. We noted that Ca^{2+} had minimal effect at 0.1 or 0.2 mM on the lipid-bound α-syn conformation, while a significant increase in β-sheet (to 26%) and β-turn (22%) content with a corresponding decrease in helical content (to 21%) was noted at 0.5 mM concentration (Figure 6, panel A, and Table 1). This observation was broadly consistent with data obtained by IR spectroscopy (Figure 6, panel B). With increasing Ca^{2+} concentrations an increased intensity was observed around ~1645 and ~1630 cm^{-1}, assigned to random coil and β-sheet structures, respectively (*51*). Although the effect we noted by IR studies was not as marked as that seen by CD data, a similar trend of Ca^{2+}-induced changes was evident, with the most pronounced effect at 0.5 mM Ca^{2+}. We, and others (*35*) note that Ca^{2+} has no effect on the secondary structure of lipid-free α-syn up to 10 mM concentration. Although Ca^{2+} has been indicated to bind lipid-free α-syn (*14*), it does not appear to induce secondary structure in the unstructured protein in aqueous solutions. However, when lipid bound via the N-terminal domain, higher Ca^{2+} levels appear to trigger β-sheet conformation in the acidic tail, possibly by facilitating extension of an already existing β-sheet-like region in the NAC domain.

Finally, to evaluate if the N-terminal and C-terminal domains from neighboring α-syn molecules are in proximity on the surface of the lipid vesicle, we examined the fluorescence emission spectra of POPC/POPA/pyrene-A11C/α-syn and POPC/POPA/pyrene-A124C/α-syn in the absence (Figure 2**)** or the presence of Ca^{2+} (Figure 5**)**. The lack of excimer fluorescence emission in the lipid-bound state in both cases is indicative of distribution of α-syn molecules over the lipid surface, with >10 Å between N-terminal ends and C-terminal ends of neighboring molecules. Further, pyrene-A11C/α-syn and pyrene-A124C/α-syn were mixed in equimolar amounts prior to lipid interaction, followed by incubation with vesicles and gel filtration as described under Materials and Methods. Fluorescence emission spectra of POPC/POPA/pyrene-A11C/α-syn/pyrene-A124C/α-syn complexes were recorded in the absence and the presence of Ca^{2+} (Figure 7). No significant excimer emission peak was noted under these conditions, indicating that the N-terminal and C-terminal domains of two neighboring molecules are not in close proximity with each other. Both in the absence and

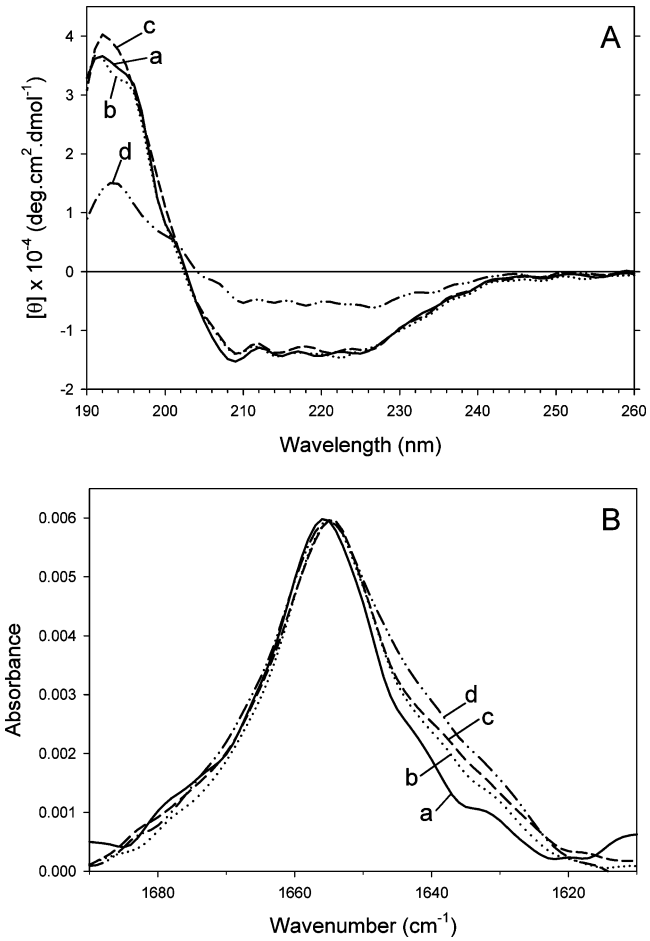

FIGURE 6: Effect of Ca^{2+} on secondary structural features of lipid-bound α-syn. CD (panel A) and amide I region of IR (panel B) spectra of POPC/POPA/α-syn complexes were recorded in the absence (a) and the presence of 0.1 mM (b), 0.2 mM (c), and 0.5 mM (d) Ca^{2+} in 5 mM HEPES, pH 7.4.

Table 1: Effect of Ca^{2+} on the Secondary Structural Content of POPC/POPA/α-Syn Complexes As Determined by CD Spectroscopy[a]

Ca^{2+} (mM)	α-helix (%)	β-sheet (%)	turn (%)	random coil (%)
0	53	11	12	25
0.1	48	13	15	24
0.2	51	13	15	21
0.5	21	26	22	30

[a] CD spectra of POPC/POPA/α-syn were recorded in 5 mM HEPES, pH 7.4, in the presence of the indicated amounts of Ca^{2+}, using a 0.05 cm cuvette. Spectra were analyzed for secondary structure content using the CDPRO analysis software (*28*) [Selcon3, ContinII, and Cdsstr with protein reference set 7 (48 proteins)].

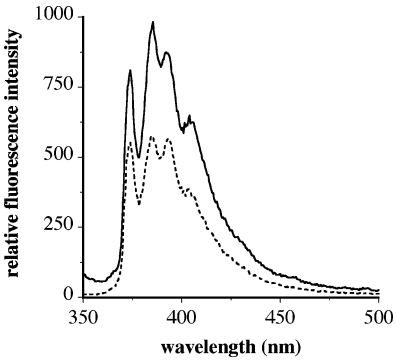

FIGURE 7: Effect of Ca^{2+} on the fluorescence emission spectra of an equimolar mixture of pyrene-A11C/α-syn and pyrene-A124/α-syn in the lipid-bound state. Pyrene-A11C/α-syn (0.5 mg) and pyrene-A124C/α-syn (0.5 mg) were mixed prior to incubation with 20 mg POPC/POPA mixtures. Lipid interaction and isolation of lipid-bound protein were carried out as described earlier. Fluorescence emission spectra of POPC/POPA/pyrene-A11C/α-syn/pyrene-A124C/α-syn in the absence (dotted line) or the presence (solid line) of 1 mM Ca^{2+} were recorded at an excitation wavelength of 340 nm.

in the presence of Ca^{2+}, the spectra appear to be a mathematical sum of the two individual spectra, i.e., of POPC/POPA/pyrene-A11C/α-syn + POPC/POPA/pyrene-A124C/α-syn. Calculations based on particle mass (226 kDa by size exclusion chromatography and 670 kDa by native PAGE analysis) and compositional analysis of the 70:1 lipid:protein ratio yield about 4−10 α-syn molecules/particle. However, since size exclusion chromatography is carried out under gentler conditions, we believe the data from these studies are more reliable, reflecting about 4−6 α-syn molecules per particle. The difference may be explained on the basis of the conformation adopted by membrane-bound α-syn or by the overall shape of the complex, which likely plays a role in determining the mobility of the lipid/protein complexes during native PAGE.

Taken together, we present a model of α-syn wherein the lipid-free protein, although unstructured, elicits a certain degree of protein−protein interaction via the N-terminal domain. The N-terminal domain initiates interaction with a suitable membrane surface, when the protein−protein interactions are replaced by protein−lipid interactions, and the α-syn molecule is anchored to the lipid surface via the N-terminal end, which adopts a helical structure. However, the presence of Ca^{2+} triggers membrane association of the C-terminal acidic tail as well, possibly by coordination, thereby bridging a direct interaction between α-syn and the membrane surface (Figure 8). It is likely that anchoring of the N-terminal domain of α-syn in the lipid particle imposes a restraint on the mobility and orientation of the acidic tail and that at optimal Ca^{2+} concentrations the NAC segment β-sheet structure extends into the C-terminal segment of the protein. Whereas the same reasoning may be applied to potential tail/tail bridging by Ca^{2+}, our fluorescence analyses are strongly in favor of Ca^{2+}-mediated α-syn tail/membrane interaction.

The scenario presented for Ca^{2+}-triggered membrane association of the α-syn acidic tail is reminiscent of Ca^{2+}-induced conformational changes in proteins such as annexin V (calcium/phospholipid binding protein). Under conditions of low Ca^{2+} levels, annexin remains cytosolic and monomeric, while at higher Ca^{2+} concentration it binds phospholipids at the surface of membranes (*52*). Our model provides molecular insights into the potential structural, physiological, and pathological role for Ca^{2+}, with lipid interaction of the acidic tail likely facilitating more aggregation of α-syn. Indeed, both the N- and C-terminal ends of α-syn have been indicated to associate with neuronal membranes in mouse cortical neurons in studies using fluorescence resonance energy transfer (*53*). Other studies indicate a high propensity for membrane-bound α-syn to aggregate and to seed aggregation of the soluble cytosolic form of the protein (*54*).

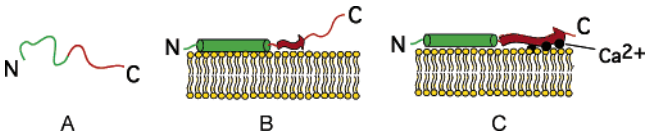

FIGURE 8: Schematic representation of the proposed Ca^{2+}-mediated interaction of the α-syn acidic tail to membranes. α-Syn is present as an unstructured protein in aqueous buffer (A). Upon lipid interaction, α-syn is anchored to the lipid surface via its N-terminal domain (represented as a green cylinder), with the C-terminal domain flapping in the surrounding aqueous milieu (B). The NAC segment is represented as a red arrow. The presence of Ca^{2+} (black dots), a key player in events occurring at the presynaptic site, triggers membrane interaction of the C-terminal acidic tail, possibly by bridging a direct interaction between the negatively charged residues on the protein and the negatively charged headgroups of the phospholipid surface (C). The acidic tail is represented as an extension of the β-strand conformation (red arrow) of the NAC segment.

In an independent experiment, we confirmed that Ca^{2+} does not cause vesicle−vesicle interaction via coordination with negatively charged headgroups of POPA in POPC/POPA/α-syn complexes by preparing complexes containing 0.1% *N*-(1-pyrenesulfonyl)-1,2-hexadecanoyl-*sn*-glycero-3-phosphoethanolamine. The presence of the pyrene moiety in the phospholipid headgroup region allows us to monitor proximity between two neighboring complexes through excimer formation. We did not note any excimer formation in these complexes under the conditions used and upon changing temperature, solution pH, or Ca^{2+} concentration (data not shown), verifying that Ca^{2+} does not promote interaction between POPC/POPA/α-syn complexes. Further, although the lifetime of protein-attached pyrene fluorophore (∼100 ns) would have allowed us to detect weak and transient interactions of the acidic tail with the membrane in the absence of Ca^{2+}, we exclude this possibility since the dose-dependent response in the band III intensity is specific to Ca^{2+}.

Negative charge clusters are often known to coordinate divalent ions such as Ca^{2+} (*55*), in conjunction with variable number of carbonyl backbone atoms and anionic headgroups of phospholipids. In the case of α-syn, the negative charge clusters in the C-terminal tail (Figure 1A) may play a role in Ca^{2+} coordination at the membrane surface. Such coordination facilitates "Ca^{2+} bridges", which are key features in the membrane association of some classes of proteins (*56*). In this state, the β-sheet content of lipid-bound α-syn increases, suggesting that it is more prone to aggregation. Alternately, the C-terminal tail may traverse the membrane bilayer with Ca^{2+} coordination of acidic residues decreasing the net charge of this segment of α-syn. It is possible that membrane juxtaposition precedes insertion and likely represents an early event in the α-syn oligomerization process. Several toxins representing the β-barrel pore-forming class

of toxins adopt a membrane-spanning β-sheet configuration (*57*). Indeed, α-syn molecules have been indicated to form annular protofibrils in solution (*58*) and in the presence of Ca^{2+} (*59*) or in a membrane environment (*58*), an observation consistent with our findings by electron microscopic analysis (data not shown). Clearly, additional factors, such as the presence of other metal ions and protein binding partners, and membrane lipid composition play critical roles in determining the structural fate of α-syn (*60*, *61*).

The high sensitivity and extinction coefficient of the pyrene fluorophore allowed us to employ very low concentrations of α-syn. Unlike NMR structural analysis, which is restricted to studying α-syn bound to micellar surface as a surrogate for membrane surface, pyrene fluorescence analysis allows use of the lipid vesicular surface, including potential use of synaptosomes, to study lipid-bound conformation of α-syn. When present in the context of the cellular milieu, α-syn encounters a more complex membrane−lipid composition, including an asymmetric distribution of phospholipids between the two leaflets. Synaptic vesicles are rich in negatively charged phospholipids such as phosphatidylserine and phosphatidic acid, reported to be located predominantly on the cytoplasmic face of synaptic vesicles (*62*), which increases the likelihood of localized elevation in Ca^{2+} levels. The Ca^{2+} levels we used in this study are in the range estimated in presynaptic microdomains (*63*, *64*), similar to that employed in other studies with α-syn (*14*, *15*, *35*, *59*). In addition, oxidative stress events associated with aging are believed to lead to an increase in intracellular Ca^{2+} levels due to increases in Ca^{2+} influx, thereby leading to severe impairment of normal physiological processes (*21*−*23*, *65*). The presynaptic membrane is therefore an ideal location for initiating pathogenesis of PD due to the abundance of α-syn, lipids, and high local concentration of Ca^{2+}(*62*, *63*).

Our studies provide structural details toward understanding the complex interplay between membranes, α-syn, and Ca^{2+} and events leading to pathogenesis of PD. Further studies are in progress to investigate the occurrence of similar structural motifs in other protein misfolding diseases or proteopathies, which will enable us to define common underlying mechanisms in the pathology of these diseases.

ACKNOWLEDGMENT

We thank Dr. Andrzej Witkowski, CHORI, for the FPLC analysis and acknowledge Dr. Susan Marqusee, University of California, Berkeley, for providing access to the CD spectrometer.

REFERENCES

1. Clayton, D. F., and George, J. M. (1998) The synucleins: a family of proteins involved in synaptic function, plasticity, neurodegeneration and disease, *Trends Neurosci. 21*, 249−254.
2. Lavedan, C. (1998) The synuclein family, *Genome Res. 8*, 871−880.
3. Duda, J. E., Lee, V. M., and Trojanowski, J. Q. (2000) Neuropathology of synuclein aggregates, *J. Neurosci. Res. 61*, 121−127.
4. Singleton, A. B., Farrer, M., Johnson, J., Singleton, A., Hague, S., Kachergus, J., Hulihan, M., Peuralinna, T., Dutra, A., Nussbaum, R., Lincoln, S., Crawley, A., Hanson, M., Maraganore, D., Adler, C., Cookson, M. R., Muenter, M., Baptista, M., Miller, D., Blancato, J., Hardy, J., and Gwinn-Hardy, K. (2003) alpha-Synuclein locus triplication causes Parkinson's disease, *Science 302*, 841.
5. Polymeropoulos, M. H., Lavedan, C., Leroy, E., Ide, S. E., Dehejia, A., Dutra, A., Pike, B., Root, H., Rubenstein, J., Boyer, R., Stenroos, E. S., Chandrasekharappa, S., Athanassiadou, A., Papapetropoulos, T., Johnson, W. G., Lazzarini, A. M., Duvoisin, R. C., Di Iorio, G., Golbe, L. I., and Nussbaum, R. L. (1997) Mutation in the alpha-synuclein gene identified in families with Parkinson's disease, *Science 276*, 2045−2047.
6. Kruger, R., Kuhn, W., Muller, T., Woitalla, D., Grabeber, M., Kosel, S., Przuntek, H., Epplen, J. T., Schols, and L., Riess, O. (1998) Ala30Pro mutation in the gene encoding alpha-synuclein in Parkinson's disease, *Nat. Genet. 18*, 106−108.
7. Bussell, R., Jr., Ramlall, T. F., and Eliezer, D. (2005) Helix periodicity, topology, and dynamics of membrane-associated alpha-synuclein, *Protein Sci. 14*, 862−872.
8. Jensen, P. H., Nielsen, M. S., Jakes, R., Dotti, G. G., and Goedert, M. (1998) Binding of alpha-synuclein to brain vesicles is abolished by familial Parkinson's disease mutation, *J. Biol. Chem. 273*, 26292−26294.
9. Jensen, P. H., Islam, K., Kenney, J., Nielsen, M. S., Power, J., and Gai, W. P. (2000) Microtubule-associated protein 1B is a component of cortical Lewy bodies and binds alpha-synuclein filaments, *J. Biol. Chem. 275*, 21500−21507.
10. Davidson, W. S., Jonas, A., Clayton, D. F., and George, J. M. (1998) Stabilization of alpha-synuclein secondary structure upon binding to synthetic membranes, *J. Biol. Chem. 273*, 9443−9449.
11. Bussell, R., Jr., and Eliezer, D. (2004) Effects of Parkinson's disease-linked mutations on the structure of lipid-associated alpha-synuclein, *Biochemistry 43*, 4810−4818.
12. Goldberg, M. S., and Lansbury, P. T., Jr. (2000) Is there a cause-and-effect relationship between alpha-synuclein fibrillization and Parkinson's disease?, *Nat. Cell Biol. 2*, E115−E119.
13. Uversky, V. N., Li, J., and Fink, A. L. (2001) Evidence for a partially folded Intermediate in α-synuclein fibril formation, *J. Biol. Chem. 276*, 10737−10744.
14. Nielsen, M. S., Vorum, H., Lindersson, E., and Jensen, P. H. (2001) Ca^{2+} binding to alpha-synuclein regulates ligand binding and oligomerization, *J. Biol. Chem. 276*, 22680−22684.
15. Narayanan, V., Guo, Y., and Scarlata, S. (2005) Fluorescence studies suggest a role for alpha-synuclein in the phosphatidylinositol lipid signaling pathway, *Biochemistry 44*, 462−470.
16. Sidhu, A., Wersinger, C., and Vernier, P. (2004) alpha-Synuclein regulation of the dopaminergic transporter: a possible role in the pathogenesis of Parkinson's disease, *FEBS Lett. 565*, 1−5.
17. Martinez, J., Moeller, I., Erdjument-Bromage, H., Tempst, P., and Lauring, B. (2003) Parkinson's disease-associated alpha-synuclein is a calmodulin substrate, *J. Biol. Chem. 278*, 17379−17387.
18. Cabin, D. E., Shimazu, K., Murphy, D., Cole, N. B., Gottschalk, W., Mellwain, K. L., Orrison, B., Chen, A., Ellis, C. E., Paylor, R., Lu, B., and Nussbaum, R. L. (2002) Synaptic vesicle depletion correlates with attenuated synaptic responses to prolonged repetitive stimulation in mice lacking alpha-synuclein, *J. Neurosci. 22*, 8797−8807.
19. Ischiropoulos, H., and Beckman, J. S. (2003) Oxidative stress and nitration in neurodegeneration: cause, effect, or association?, *J. Clin. Invest. 111*, 163−169.
20. Schulz, J., Lindenau, J., Seyfried, J., and Dichgans, J. (2000) Glutathione, oxidative stress and neurodegeneration, *Eur. J. Biochem. 267*, 4904−4911.
21. Cuschieri, J., Bulger, E., Garcia, I., and Maier, R. V. (2005) Oxidative-induced calcium mobilization is dependent on annexin VI release from lipid rafts, *Surgery 138*, 158−164.
22. Denisova, N., Strain, J., and Joseph, J. A. (1997) Oxidant injury in PC-12 cells−a possible model of calcium "dysregulation" in aging: II. Interactions with membrane lipids, *J. Neurochem. 69*, 1259−1266.
23. Huang, C.-L., Huang, N.-K., Shyue, S.-K., and Chern, Y. (2003) Hydrogen peroxide induces loss of dopamine transporter activity: a calcium dependent oxidative mechanism, *J. Neurochem. 86*, 1247−1259.
24. Narayanaswami, V., Szeto, S. S., and Ryan, R. O. (2001) Lipid association-induced N- and C-terminal domain reorganization in human apolipoprotein E3, *J. Biol. Chem. 276*, 37853−37860.
25. Sahoo, D., Weers, P. M., Ryan, R. O., and Narayanaswami, V. (2002) Lipid-triggered conformational switch of apolipophorin III helix bundle to an extended helix organization, *J. Mol. Biol. 321*, 201−214.
26. Sahoo, D., Narayanaswami, V., Kay, C. M., and Ryan, R. O. (2000) Pyrene excimer fluorescence: a spatially sensitive probe

to monitor lipid-induced helical rearrangement of apolipophorin III, *Biochemistry 39*, 6594−6601.
27. Eftink, M. R., and Ghiron, C. A. (1976) Exposure of tryptophanyl residues in proteins. Quantitative determination by fluorescence quenching studies, *Biochemistry 15*, 672−680.
28. Sreerama, N., Venyaminov, S. Y., and Woody, R. W. (2000) Estimation of protein secondary structure from circular dichroism spectra: inclusion of denatured proteins with native proteins in the analysis, *Anal. Biochem. 287*, 243−251.
29. Haugland, R. P. (2005) *The Handbook. A Guide to Fluorescent Probes and Labeling Technologies*, 10th ed., Invitrogen Corp., Carlsbad, Ca.
30. Tedeschi, C., Muhwald, H., and Kirstein, S. (2001) Polarity of layer-by-layer deposited polyelectrolyte films as determined by pyrene fluorescence, *J. Am. Chem. Soc. 123*, 954−960.
31. Dong, D. C., and Winnick, M. A. (1982) The PY scale of solvent polarities−Solvent effects on the vibronic fine structure of pyrene fluorescence and empirical correlations with Et-value and Y-value, *Photochem. Photobiol. 35*, 17−21.
32. Karpovich, D. S., and Blanchard, G. J. (1995) Relating the polarity-dependent fluorescence response of pyrene to vibronic coupling. Achieving a fundamental understanding of the *py* polarity scale, *J. Phys. Chem. 99*, 3951−3958.
33. Winnick, F. M. (1993) Photophysics of preassociated pyrenes in aqueous polymer solutions and in other organized media, *Chem. Rev. 93*, 587−614.
34. Aricha, B., Fishov, I., Cohen, Z., Sikron, N., Pesakhov, S., Khozin-Goldberg, I., Dagan, R., and Porat, N. (2004) Differences in membrane fluidity and fatty acid composition between phenotypic variants of *Streptococcus pneumoniae*, *J. Bacteriol. 186*, 4638−4644.
35. Weinreb, P. H., Zhen, W., Poon, A. W., Conway, K. A., and Lansbury, P. T., Jr. (1996) NACP, a protein implicated in Alzheimer's disease and learning, is natively unfolded, *Biochemistry 35*, 13709−13715.
36. Jung, K., Jung, H., and Kaback, H. R. (1994) Dynamics of lactose permease of *Escherichia coli* determined by site-directed fluorescence labeling, *Biochemistry 33*, 3980−3985.
37. Hammarstrom, P., Kalman, B., Jonsson, B. H., and Carlsson, U. (1997) Pyrene excimer fluorescence as a proximity probe for investigation of residual structure in the unfolded state of human carbonic anhydrase II, *FEBS Lett. 420*, 63−68.
38. Zhao, M., Zen, K. C., Hubbell, W. L., and Kaback, H. R. (1999) Proximity between Glu126 and Arg144 in the lactose permease of *Escherichia coli*, *Biochemistry 38*, 7407−7412.
39. Perrin, R. J., Woods, W. S., Clayton, D. F., and George, J. M. (2000) Interaction of human α-synuclein and Parkinson's disease variants with phospholipids. Structural analysis using site-directed mutagenesis, *J. Biol. Chem. 275*, 34393−34398.
40. Perrin, R. J., Woods, W. S., Clayton, D. F., and George, J. M. (2001) Exposure to long chain polyunsaturated fatty acids triggers rapid multimerization of synucleins, *J. Biol. Chem. 276*, 41958−41962.
41. Jao, C. C., Der-Sarkissian, A., Chen, J., and Langen, R. (2004) Structure of membrane-bound alpha-synuclein studied by site-directed spin labeling, *Proc. Natl. Acad. Sci. U.S.A. 101*, 8331−8336.
42. Garidel, P., Johann, C., and Blume, A. (1997) Nonideal mixing and phase separation in phosphatidylcholine-phosphatidic acid mixtures as a function of acyl chain length and pH, *Biophys. J. 72*, 2196−2210.
43. Neher, E. (1998) Usefulness and limitations of linear approximations to the understanding of Ca^{2+} signals, *Cell Calcium 24*, 345−357.
44. Maeda, H., Ellis-Davies, G. C. R., Ito, K., Miyashita, Y., and Kasai, H. (1999) Supralinear Ca^{2+} signaling by cooperative and mobile Ca^{2+} buffering in Purkinje neurons, *Neuron 24*, 989−1002.
45. Drury, J., and Narayanaswami, V. (2005) Examination of lipid-bound conformation of apolipoprotein E4 by pyrene excimer fluorescence, *J. Biol. Chem. 280*, 14605−14610.
46. Abrams, F. S., and London, E. (1992) Calibration of the parallax fluorescence quenching method for determination of membrane penetration depth: refinement and comparison of quenching by spin-labeled and brominated lipids, *Biochemistry 31*, 5312−5322.
47. Heuck, A. P., Tweten, R. K., and Johnson, A. E. (2003) Assembly and topography of the prepore complex in cholesterol-dependent cytolysins, *J. Biol. Chem. 278*, 31218−31225.
48. Cawthern, K. M., Narayan, M., Chaudhuri, D., Permyakov, E. A., and Berliner, L. J. (1997) Interactions of a-lactalalbumin with fatty acids and spin label analogs, *J. Biol. Chem. 272*, 30812−30816.
49. Lücke, C., Gantz, D. L., Klimtchuk, E., and Hamilton, J. A. (2006) Interactions between fatty acids and α-synuclein, *J. Lipid Res.* (in press) (published online ahead of print May 10, 2006).
50. Raussens, V., Drury, J., Forte, T. M., Choy, N., Goormaghtigh, E., Ruysschaert, J. M., and Narayanaswami, V. (2005) Orientation and mode of lipid-binding interaction of human apolipoprotein E C-terminal domain, *Biochem. J. 387*, 747−754.
51. Goormaghtigh, E., Cabiaux, V., and Ruysschaert, J. M. (1994) Determination of soluble and membrane protein structure by Fourier transform infrared spectroscopy. III. Secondary structures, *Subcell. Biochem. 23*, 405−450.
52. Luecke, H., Chang, B. T., Mailliard, W. S., Schlaepfer, D. D., and Haigler, H. T. (1995) Crystal structure of the annexin XII hexamer and implications for bilayer insertion, *Nature 378*, 512−515.
53. McLean, P. J., Kawamata, H., Ribich, S., and Hyman, B. T. (2000) Membrane association and protein conformation of alpha-synuclein in intact neurons. Effect of Parkinson's disease-linked mutations, *J. Biol. Chem. 275*, 8812−8816.
54. Lee, H.-J., Choi, C., and Lee, S.-L. (2002) Membrane-bound α-synuclein has a high aggregation propensity and the ability to seed the aggregation of the cytosolic form, *J. Biol. Chem. 277*, 671−678.
55. Zhu, Z. Y., and Karlin, S. (1996) Clusters of charged residues in protein three-dimensional structures, *Proc. Natl. Acad. Sci. U.S.A. 93*, 8350−8355.
56. Swairjo, M. A., Concha, N. O., Kaetzel, M. A., Dedman, J., and Seaton, B. A, (1995) Ca(2+)-bridging mechanism and phospholipid headgroup recognition in the membrane-binding protein annexin V, *Nat. Struct. Biol. 2*, 968−974.
57. Heuck, A. P., Tweten, R. K., and Johnson, A. E. (2001) Beta-barrel pore-forming toxins: intriguing dimorphic proteins, *Biochemistry 40*, 9065−9073.
58. Ding, T. T., Lee, S. J., Rochet, J. C., and Lansbury, P., Jr. (2002) Annular alpha-synuclein protofibrils are produced when spherical protofibrils are incubated in solution or bound to brain-derived membranes, *Biochemistry 41*, 10209−10217.
59. Lowe, R., Pountney, D. L., Jensen, P. H., Gai, W. P., and Voelcker, N. H. (2004) Calcium(II) selectively induces α-synuclein annular oligomers via interaction with the C-terminal domain, *Protein Sci. 13*, 3245−3252.
60. Uversky, V. N., Li, J., and Fink, A. L. (2001) Metal-triggered structural transformations, aggregation, and fibrillation of human α-synuclein. A possible molecular link between Parkinson's disease and heavy metal exposure, *J. Biol. Chem. 276*, 44284−44296.
61. Zhu, M., Li, J., and Fink, A. L. (2003) The association of alpha-synuclein with membranes affects bilayer structure, stability, and fibril formation, *J. Biol. Chem. 278*, 40186−40197.
62. Michaelson, D. M., Barkai, G., and Barenholz, Y. (1983) Asymmetry of lipid organization in cholinergic synaptic vesicle membranes, *Biochem. J. 211*, 155−162.
63. Llinas, R., Sugimori, M., and Silver, R. B. (1995) The concept of calcium concentration microdomains in synaptic transmission, *Neuropharmacology 34*, 1443−1451.
64. Llinas, R., Sugimori, M., and Silver, R. B. (1992) Microdomains of high calcium concentration in a presynaptic terminal, *Science 256*, 677−679.
65. Hoyal, C. R., Thomas, A. P., and Forman, H. J. (1996) Hydroperoxide-induced increases in intracellular calcium due to annexin VI translocation and inactivation of plasma membrane Ca^{2+}-ATPase, *J. Biol. Chem. 271*, 29205−29210.

BI060939I